NANO LETTERS

pubs.acs.org/NanoLett

Letter

Thermophilic Behavior of Heat-Dissociative Coacervate Droplets

Youngsun Kim and Yuebing Zheng*

Cite This: *Nano Lett.* 2024, 24, 15964−15972

Read Online

ACCESS | Metrics & More | Article Recommendations | Supporting Information

ABSTRACT: In exploring the genesis of life, liquid−liquid phase-separated coacervate droplets have been proposed as primitive protocells. Within the hydrothermal hypothesis, these droplets would emerge from molecule-rich hot fluids and thus be subjected to temperature gradients. Investigating their thermophoretic behavior can provide insights into protocell footprints in thermal landscapes, advancing our understanding of life's origins. Here, we report the thermophilic behavior of heat-dissociative droplets, contrary to the intuition that heat-associative condensates would prefer hotter areas. This aspect implies the preferential presence of heat-dissociative primordial condensates near hydrothermal environments, facilitating molecular incorporation and biochemical syntheses. Additionally, our investigations reveal similarities between thermophoretic and electrophoretic motions, dictated by molecular redistribution within droplets due to their fluid nature, which necessitates revising current electrophoresis frameworks for surface charge characterization. Our study elucidates how coacervate droplets navigate thermal and electric fields, reveals their thermal-landscape-dependent molecular characteristics, and bridges foundational theories of early life: the hydrothermal and condensate-as-protocell hypotheses.

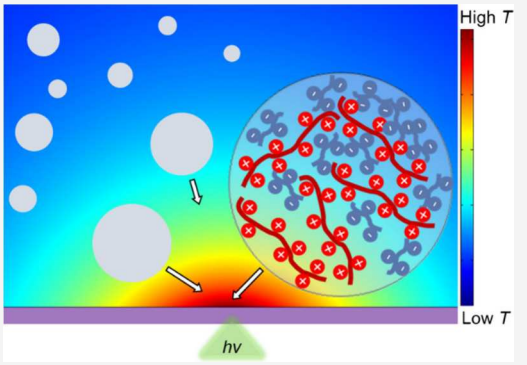

KEYWORDS: *thermophoresis, liquid−liquid phase separation, origin of life, coacervate droplets, polyelectrolytes*

Recent evidence has indicated that liquid−liquid phase separation (LLPS) plays a crucial role in forming membrane-less subcellular organelles and is involved in cellular processes.[1−3] Unlike typical liquid-in-liquid systems, which are separated by surface-active materials, such as surfactants and lipids, a homogeneous aqueous solution of macromolecules can undergo LLPS. This results in a discrete solute-rich phase (i.e., coacervate droplets or condensates) within a dilute solution when the solute concentration exceeds a critical point. The simplicity of this phase behavior, coupled with its ability to spatially localize and selectively accommodate molecules for biochemical synthesis,[4−9] has suggested that LLPS-driven droplets could be a primitive form of protocells in the early emergence of life, from which the evolution to organized and functional entities would initiate. The primary mechanism behind LLPS is multivalent molecular interactions through which molecules form an entangled network, creating a relatively hydrophobic core. One of the key parameters that influences LLPS is temperature. Many biomolecular condensates exhibit a heat-dissociative characteristic, featured by an upper critical solution temperature (UCST) above which droplets dissolve back into a homogeneous solution, due to underlying thermally dissociative interactions such as electrostatic and hydrogen bonding.[3,10] Some exceptions have been found that coacervates based on nucleotide−multivalent ion and hydrophobic interactions exhibit a lower critical solution temperature (LCST).[3,11] Moreover, the coacervate phase remains metastable before transforming into more solid-like condensates[1,3,12] and is unstable in the case of droplets formed from loosely interacting molecules (e.g., short-chain scaffold molecules[13−15]).

The origin of life has long been believed to be from hydrothermal environments in the deep ocean.[16,17] These environments are characterized by high temperatures, pressures, and molecular concentrations, conditions under which simple molecules engage in activity-driven chemical reactions that produce prebiotic molecules and polymers.[16−19] The hydrothermal environments are inherently accompanied by temperature gradients. The temperature of the water stream from deep-sea hydrothermal vents ranges from 60 to >400 °C. When the LLPS-driven molecular condensation is aligned with the hydrothermal hypothesis, earlier condensates would be formed in molecule-rich hot liquids and exposed to temperature gradients. At first glance, one might expect that heat-associative condensates favorably exist in hydrothermal environments. However, primitive molecular condensates, likely composed of short and simple molecules, might have loosely bound networks and heat-dissociative properties. In this context, delving into the thermophoretic actions of heat-

Received: June 28, 2024
Revised: November 4, 2024
Accepted: November 13, 2024
Published: November 22, 2024

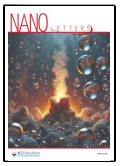

https://doi.org/10.1021/acs.nanolett.4c03058
Nano Lett. 2024, 24, 15964−15972

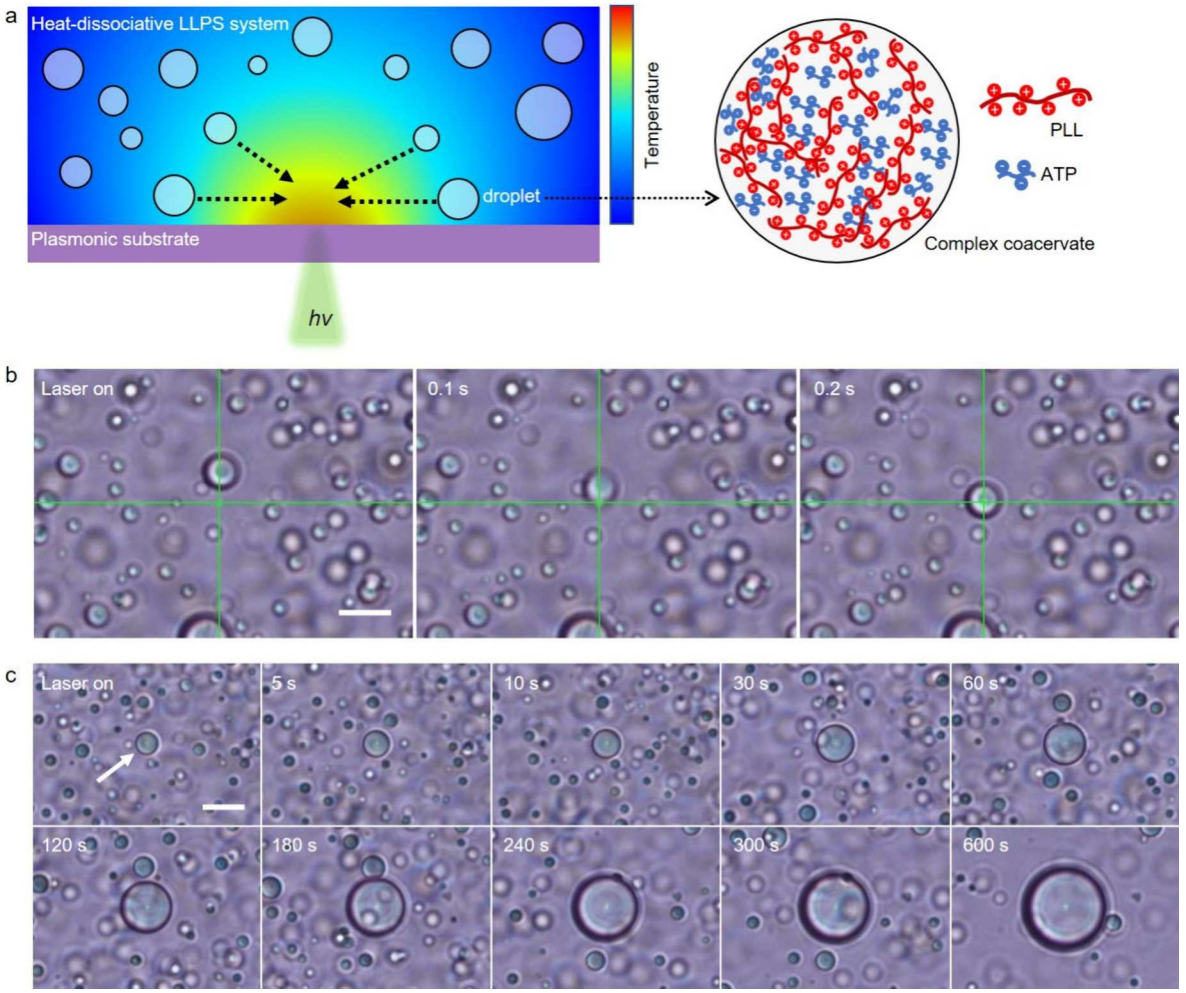

Figure 1. Thermophilic behavior of heat-dissociative coacervate droplets. (a) Schematic illustration of droplet motion under an optically generated temperature field (532 nm laser) and electrostatically complexed droplet. (b) Microscopic images of a droplet trapped by a laser (0.51 mW). (c) Temporal evolution of a thermally trapped droplet under continuous exposure to the laser (0.51 mW; scale bars: 10 μm).

responsive condensates could offer a glimpse into protocells' possible trajectories across thermal environments, enriching our comprehension of life's beginnings and governing principles.

While the core region of coacervate droplets has been extensively studied, the interface between the dilute and dense phases remains somewhat elusive,[20−22] despite observations of interfacial phenomena—such as the localization of molecules, liposomes, and bacteria,[21,23−26] along with interfacial flow-driven LLPS dynamics[27−29]—highlighting its significance in understanding the behavior of coacervate droplets.[12,30] One of the commonly investigated interfacial properties is the surface charge of droplets, derived from the zeta potential measured by electrophoresis (primarily through dynamic light scattering methods), because the sign and magnitude of the surface charge can reflect the molecular arrangement at the interface.[22,30−36] Although the fusion dynamics of some biological condensates has aligned with their zeta potentials,[34] a controversial observation has been reported for the relationship between colloidal stability and zeta potential: higher stability at lower zeta potentials.[33] This discrepancy may stem from the presumption that droplets are solid colloidal particles when zeta potentials are derived. The fluid nature of droplets implies that charge-carrying components can migrate under an external electric field, potentially inducing charge and composition gradients within and surrounding the droplets, thus affecting their electrophoretic properties.[15,37] Therefore, revisions in the current electrophoresis methodology are required for a better understanding of the molecular nature of coacervate droplets.

In this study, we explore the behavior of heat-responsive coacervate droplets under a local temperature gradient. We reveal that heat-dissociative coacervate droplets actively navigate through temperature gradients, demonstrating a distinct thermophilic nature. This attribute underscores its potential significance in the origins of life, especially in the cellular evolution of primitive structures, as it indicates a natural affinity of heat-dissociative primordial condensates for warm, nutrient-dense locales where the probability of further molecule assimilation and reaction significantly increases. In addition, we present the critical role of molecular reallocation within the droplets in interpreting their thermophoretic and electrophoretic motions, prompting a revision of current analytical frameworks for electrophoresis involving the surface charge characterization of coacervate droplets. By delineating a pathway for coacervate droplets and underlying molecular characteristics within thermal fields, our work fosters a connection between two fundamental theories proposed for the separate stages of life emergence, i.e., the hydrothermal

https://doi.org/10.1021/acs.nanolett.4c03058
Nano Lett. 2024, 24, 15964−15972

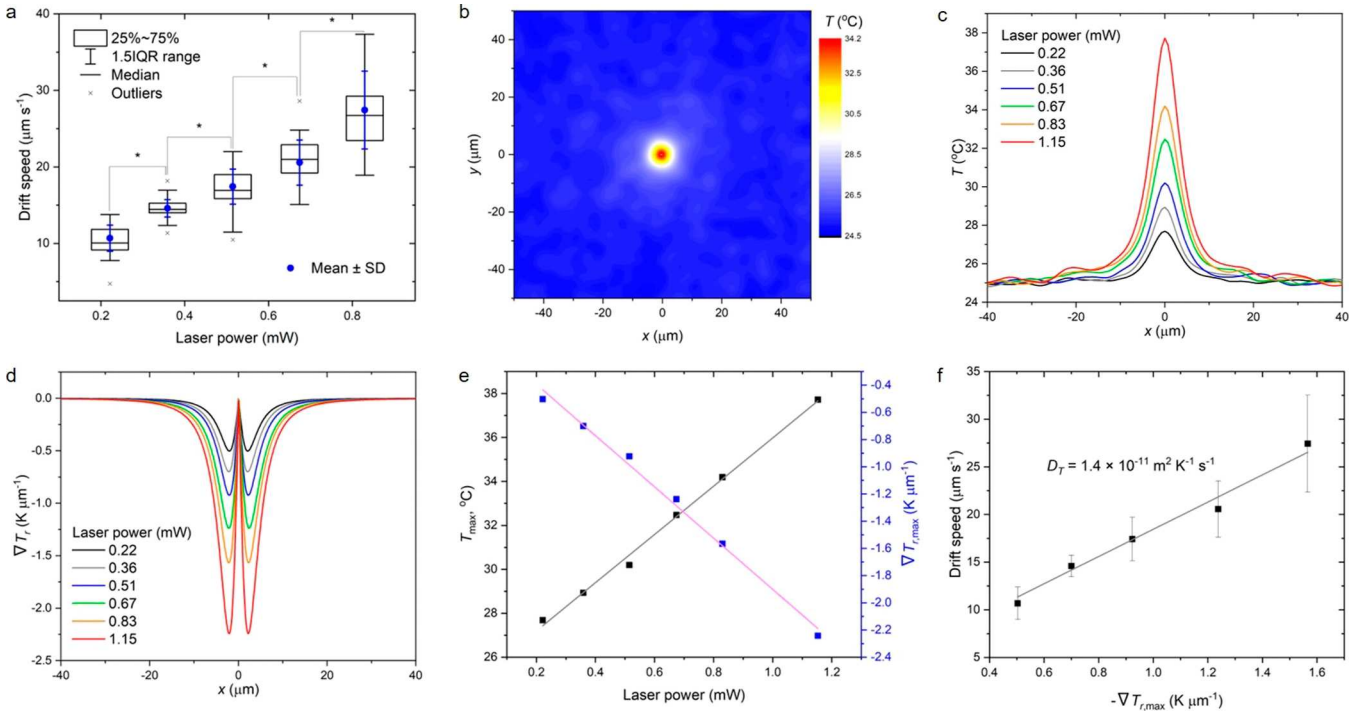

Figure 2. Optical power-dependent thermophoretic and thermal characteristics. (a) Drift speed of coacervate droplets at varying laser powers. The boxes indicate the upper and lower quartiles with the median (center line), and the whiskers indicate the 1.5 interquartile range (IQR) (n = 25, cross symbols: outliers). p-Values are statistically significant according to Student's t-test; *p < 0.05. The blue scatter plots show mean ± standard deviation (SD) without outliers. (b) Temperature map of a plasmonic substrate at 0.83 mW laser power. (c) Temperature and (d) in-plane temperature gradient profiles measured at varying laser powers. The in-plane temperature gradient is defined as $\partial T/\partial r$, where r is the distance from the beam center. (e) Maximum temperature and maximum negative temperature gradient with respect to laser power (solid lines: linear fit, R^2 > 0.95). (f) Drift speed as a function of maximum temperature gradient (solid line: linear fit, R^2 > 0.95).

hypothesis for prebiotic synthesis and the condensate-as-protocell hypothesis for cellular evolution.

Among various coacervate systems, we selected a binary charge-complexed coacervate model consisting of poly-L-lysine (PLL) and adenosine triphosphate (ATP) for its soft and heat-dissociative characteristics[13,15,22,38] (Table S1 and Figure S1). This system exhibits UCSTs that vary with salt concentrations, displaying a lower UCST for higher salt concentrations.[15] The coacervate sample was prepared at 5 mM PLL (on a monomer basis), 5 mM ATP, and 200 mM NaCl in HEPES buffer (see Methods). The total sample volume of 4 mL yielded 15 μL of a coacervate phase (Figure S2), and the concentration of PLL (monomer basis) and ATP in the coacervate phase was 1.333 and 0.213 M, respectively. The water content of the coacervate phase was measured as 76 wt % by freeze-drying the separated coacervate phase. As depicted in Figure 1a, a microscale temperature gradient is generated by focusing a continuous wave (CW) laser on a plasmonic substrate (see Figure S3 for substrate preparation and structural and optical characterizations) using an objective lens with a numerical aperture (NA) of 0.5 (Figure S4). Upon laser illumination on a sample-loaded substrate, dispersed coacervate droplets drift toward and are trapped at the beam center (Figure 1b and Movie S1). It was also observed that a trapped droplet could be transported by moving the sample stage relative to the laser beam (Movie S1). With continuous laser illumination, a trapped droplet grows by successively merging with multiple droplets attracted to the beam (Figure 1c and Movie S2). The thermally trapped droplet remained trapped for several hours (Figure S5), despite the colloidal instability of the PLL-ATP droplets (Figures S6 and S7). The drift speed of the droplets did not show a size dependence (Figure S8), unlike the size-dependent speed of coacervate droplets under an electric field.[33,39] Interestingly, under the optothermal temperature gradient, polydiallyldimethylammonium (PDDA)-ATP coacervate droplets were repelled (Movie S3). The PDDA-ATP system is known to be relatively heat-resistant, stable up to 85 °C.[35] Given that the laser was used to generate heat, we also experimented with optical trapping to assess its contribution to the motion of the droplets. When PLL-ATP droplets were exposed to the same laser without the plasmonic substrate, no optical trapping of the droplets was observed (Movie S4), which was attributed to the loosely focused laser beam with the low-NA objective lens. Consequently, we ruled out the optical trapping effect, confirming that the movement of the droplets is predominantly governed by the thermal gradient.

Figure 2a shows the drift speeds of droplets at varying laser powers. With an increase in laser power, higher speeds were observed, indicating that the thermal gradient acts as the driving force behind the motion of the droplets. At laser powers below 0.22 mW, the thermophoretic motion of droplets was unobservable due to a weak driving force insufficient to overcome Brownian motion. Additionally, a portion of trapped droplets dissolved at the beam center when using laser powers above 1.15 mW (Figure S9), suggesting the heat-dissociative nature of the droplets. The temperature profile was measured as axisymmetric about the beam center (Figure 2b), with the maximum temperature, T_{max}, ranging from around 28 to 38 °C (Figure 2c). The in-plane temperature gradient, ∇T_r, has its negative maximum at 2

https://doi.org/10.1021/acs.nanolett.4c03058
Nano Lett. 2024, 24, 15964−15972

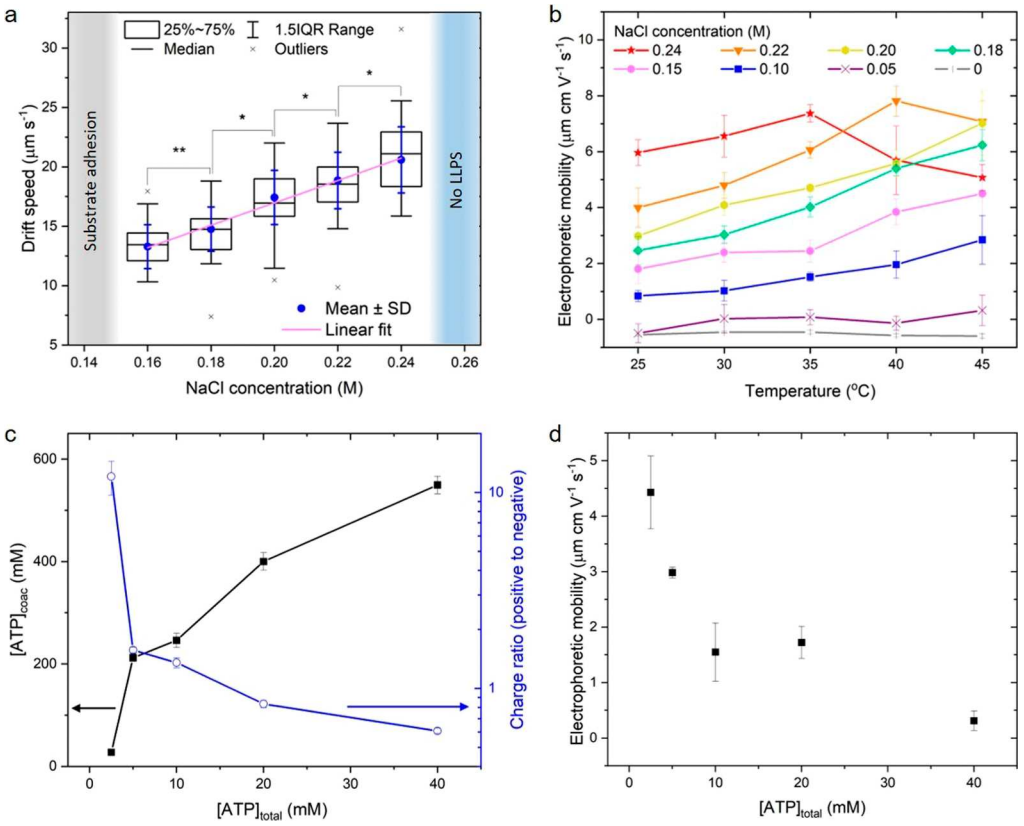

Figure 3. Composition-dependent thermophoretic and electrophoretic properties. (a) Thermophoretic drift speed of PLL-ATP droplets at varying NaCl concentrations (laser power: 0.51 mW). The boxes indicate the upper and lower quartiles with the median (center line), and the whiskers indicate the 1.5 interquartile range (IQR) (n = 25, cross symbols: outliers). p-Values are statistically significant according to Student's t-test; $^*p <$ 0.05, except $^{**}p$ = 0.059. The blue scatter plots show mean ± SD without outliers, and the blue line indicates a linear fit ($R^2 > 0.95$). (b) Temperature-dependent electrophoretic mobility of droplets at varying NaCl concentrations (mean ± SD, n = 5). (c) ATP concentration, $[ATP]_{coac}$, and charge ratio in the coacervate phase at varying total ATP concentrations, $[ATP]_{total}$ (mean ± SD, n = 3). (d) Electrophoretic mobility of droplets at varying ATP concentrations (mean ± SD, n = 5).

μm from the beam center (Figure 2d). The negative sign corresponds to the temperature gradient directed toward the beam center. T_{max} and $-\nabla T_r$ were found to be proportional to the laser power (Figure 2e), given the fixed beam geometry. The thermophoretic drift velocity can be expressed as $\mathbf{u}_{th} = -D_T \nabla T$, where D_T is the thermodiffusion coefficient. D_T was derived as 1.4×10^{-11} m^2 K^{-1} s^{-1} using the maximum ∇T_r (Figure 2f), which is an order of magnitude higher than that of solid microparticles.[40] This difference implies the existence of an additional driving force that arises from the liquid-like nature of the droplets.

The ionic strength in this system works against LLPS by screening the charge complexation between polycations and polyanions,[13,15,35] thus weakening the structural rigidity of the droplets. LLPS is halted above a critical salt concentration threshold (0.25 M NaCl). As the concentration of NaCl increases, a linear increase in drift speeds was observed (Figure 3a). Thus, the thermodiffusion coefficient of this system, D_T, is a function of ionic strength, with a proportionality constant of 1.0×10^{-7} m^5 s^{-1} K^{-1} mol^{-1}. Notably, at concentrations below 0.15 M NaCl, droplets were drawn toward the beam but adhered to the substrate before reaching the beam center (Movie S5). At 0 M added NaCl, numerous droplets immediately wetted the substrate in an irregular shape (Figure S10), implying an increased density and viscosity resulting from the intensified electrostatic interaction between PLL and ATP.[13,41] This observation is consistent with the relatively heat-resistant characteristic of the system.[15] Under these conditions, the remaining colloidal droplets were not able to be capped by the optothermal field (Movie S5).

To decipher the thermophoretic motion in relation to the behavior of the charged constituents, electrophoretic studies were conducted. Traditionally, surface charge characterization for coacervate droplets relies on zeta potential measurements via electrophoresis, assuming that the droplets behave as solid colloidal particles. Reported zeta potentials show considerable variation (4−60 mV in absolute values), which have been employed to describe the sign and extent of the surface charge. However, inconsistencies arise when correlating the zeta potential with the colloidal stability.[33] Our measurements also revealed such inconsistencies. Briefly, the zeta potentials of the PLL-ATP droplets at 0 and 0.2 M NaCl were −5 and +80 mV, respectively, under the Smoluschowski approximation. Typically, at higher salt concentrations, ions screen the surface charge of a colloidal object, reducing the zeta potential by shrinking the Debye layer. This observation sharply contrasts with our measured zeta potential values. The Smoluchowski or Huckel approximation, used to convert electrical responses into zeta potentials for rigid particles, fails for liquid colloids where internal molecules and charges are mobile.[37,39,42,43] In addition to the electrostatic effect exerted by the applied electric field, the rearrangement of charged species in a liquid and the concomitant redistribution of ions in the electrical double layer lead to a retarding force called electroosmosis.

https://doi.org/10.1021/acs.nanolett.4c03058
Nano Lett. 2024, 24, 15964−15972

Furthermore, the redistribution of droplet components induces composition variation along the droplet−liquid interface, which generates a Marangoni flow along the interface. Due to this complexity, the zeta potential characterization under the solid-particle approximation (i.e., assuming fixed surface charge and electrostatic force) does not accurately reflect the effective surface charge of droplets.

However, the electrophoretic measurement still provides important information, namely, electrophoretic mobility, which is defined as the electrophoretic velocity relative to the applied electric field. These raw data, before being converted to the zeta potential, essentially reflect how fast and in what direction colloidal objects move under the electric field due to all the above-mentioned effects. Our observations showed distinct trends in electrophoretic mobility with ionic strength. As shown in Figure 3b, the electrophoretic mobility demonstrates a clear trend of increasing with higher NaCl concentrations. Thermophilic droplets prepared at higher NaCl concentrations exhibit relatively high mobilities (e.g., 3−8 μm·cm V^{-1} s^{-1} for 0.2 M NaCl) that escalate with the temperature. The positive mobility values indicate movement toward the negative electrode (cathode in electrophoresis). It is observed that the mobility trend reverses at 40 and 35 °C for 0.22 and 0.24 M NaCl, respectively, a phenomenon linked to the critical temperature shifting to lower values at elevated salt concentrations.[15] In contrast, at 0 M NaCl, droplets show a negative mobility of −0.5 μm·cm V^{-1} s^{-1}, unaffected by temperature changes. Indeed, there is a similarity between the electrophoretic and thermophoretic behaviors, with more thermophilic droplets being more electrically responsive. This analogy suggests common underlying dynamics between the electrophoresis and thermophoresis of droplets.

In the electrophoresis of liquid particles, the Marangoni effect can be either parallel or antiparallel to electrostatic motion induced by an applied electric field, while electro-osmosis always counteracts electrostatic motion. Given that the electroosmotic force (induced) cannot exceed the electrostatic force (applied), as well as the sign inversion of electrophoretic mobility between 0 and 0.2 M NaCl samples, the Marangoni effect is the only plausible dominant driving force. We assumed that variation in the net charge of droplets across different ionic strengths is negligible, given the same concentrations of PLL and ATP. To modify the net charge of droplets, the concentration of ATP was adjusted while the PLL concentration was kept constant (5 mM, monomer basis). The ATP concentration within the coacervate phase was determined using UV−vis spectroscopy (see Methods and Figure S2), and the positive-to-negative charge ratio was calculated. Figure 3c illustrates the ATP concentration in the coacervate phase, $[ATP]_{coac}$, and the coacervate charge ratio with respect to the total ATP concentration, $[ATP]_{total}$. $[ATP]_{coac}$ increases as $[ATP]_{total}$ rises, and consequently, the positive-to-negative charge ratio of the coacervate phase diminishes with increasing $[ATP]_{total}$, reversing the net charge of the coacervate phase from positive to negative when $[ATP]_{total}$ reaches 10−20 mM. Across all tested ATP concentrations, the turbidity of the samples rapidly declines over time (see Methods and Figure S7), demonstrating the unstable nature of these droplets regardless of their net charge.

At higher ATP concentrations, reduced electrophoretic mobilities and increased thermophoretic mobilities were observed (Figure 3d and Figure S11, respectively), implying the presence of the Marangoni effect. Droplets acquire more negative charges with ATP, enhancing electrostatic responses toward the cathode during electrophoresis (negative mobility). As a result, the positive electrophoretic mobility decreases with increasing ATP concentrations from 4.5 to 0.3 μm·cm V^{-1} s^{-1}; however, the sign of electrophoretic mobility does not shift to negative values. In other words, even the droplets with negative net charges (i.e., at 20−40 mM ATP) continue moving toward the negative electrode. This movement suggests that the Marangoni effect influences the droplets, propelling them toward the cathode while being compensated by the counteracting electrostatic effect of increasing negative charge content. Taking the factors together, the electrophoretic motion of droplets at low and high salt concentrations is illustrated in Figure 4. In the presence of Na^+ and Cl^-, the interaction between ATP and PLL is weakened, allowing the polyelectrolytes within droplets to be relatively mobile and separated within a droplet by an applied electric field. From the signs of electrophoretic mobility, this charge separation lowers the interfacial tension in PLL-rich areas and increases it in ATP-rich areas, generating Marangoni flow that drives the droplet toward the cathode. Without Na^+ and Cl^-, polyelectrolytes remain tightly entangled, resulting in electrical unresponsiveness due to less profound charge separation. The influence of NaCl on the PLL−ATP interaction is further evidenced by turbidity measurements, showing that turbidity drops at higher NaCl concentrations (see the Methods and Figure S7). This decrease suggests that coacervation is inhibited at high salt concentrations.[15] For heat-resistant PDDA-ATP droplets, which exhibit thermophobic motion (Movie S3), the electrophoretic mobility remained relatively unchanged across temperatures (Figure S12), attributable to a rigid PDDA-ATP network.

Leveraging insights from electrophoresis, we interpreted the thermophoretic motion of the droplets. Typically, the interfacial tension between coacervate droplets and the solution ranges from 0.1−100 μN/m[38] and approaches zero near critical points[2,44,45] such as the critical polyelectrolyte concentration, critical solution temperature, and critical salt concentration. Since the PLL-ATP system exhibits a UCST characteristic, the interfacial tension diminishes in high-temperature regions (Note S1), resulting in Marangoni flow. This effect is illustrated in Figure 4a, which shows a simulated cross-sectional flow profile for a single PLL-ATP droplet in a 0.2 M NaCl solution under an optically generated thermal field (see Note S1 and Figure S13 for simulation details). The temperature-driven interfacial tension gradient along the droplet surface generates a slip velocity field around the droplet (cf. significantly weak internal flow due to the higher viscosity of the droplet), leading to the drag of the droplet toward the hot spot at the origin.[46−49] The net drift speed of the droplet was calculated as 2.3 μm s^{-1} by averaging the tangential flow velocities along the interface, which is lower than the thermophoretic speed of 17 μm s^{-1} (Figure 2a, at 0.51 mW). This discrepancy implies the existence of additional mechanisms that promote the motion of the droplet, which we inferred from the thermophoretic properties of the molecules. It was noted that the flow speed driven by natural convection is negligible compared to that of the Marangoni flow (Figure S14).

Molecules migrate under a temperature gradient, with the degree and direction of migration influenced by factors such as molecular size, chemical structure, and conformation.[18,50,51] Although the underlying mechanism of molecular thermal

https://doi.org/10.1021/acs.nanolett.4c03058
Nano Lett. 2024, 24, 15964−15972

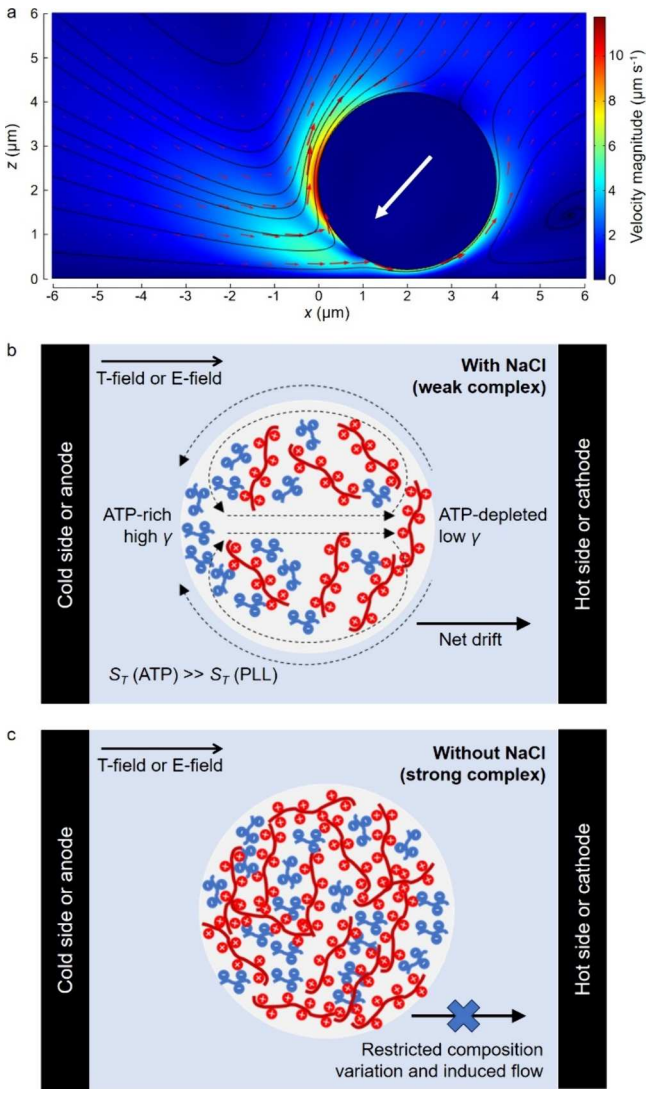

Figure 4. Flow dynamics and mechanism of thermophoretic and electrophoretic motion of a coacervate droplet. (a) Simulated cross-sectional flow profile for a PLL-ATP droplet in a 0.2 M NaCl solution under an optically generated thermal field. The origin (0, 0) is the hot spot where the laser beam is focused. The *z*-axis is the beam axis. The black solid lines and red arrows represent streamlines and velocity vectors, respectively. The white arrow indicates the propulsion direction of the droplet. (b) With NaCl, charge complexation between ATP and PLL is weakened, allowing polyelectrolytes to be redistributed within the droplet along a temperature or electric field. Subsequently, composition-driven interfacial flows are generated, driving the droplet toward a hot region or cathode in thermophoresis and electrophoresis, respectively. (c) Without NaCl, stronger complexation reduces the mobility of the charge-carrying species, so effective composition variation does not occur to drive the droplet along the temperature and electric fields. For electrophoresis in (b) and (c), the cathode and anode correspond to the negative and positive electrodes, respectively.

migration is not fully understood, the thermophoretic properties of molecules can be characterized by the Soret coefficient (S_T). The S_T of PLL was calculated to be 3.5×10^{-3} K^{-1} (Note S2), indicating thermophobic migration due to the positive S_T. The S_T of ATP was estimated as 2.0×10^{-2} K^{-1}, based on the molecular weight-dependent S_T for single-stranded RNA, which is significantly higher than PLL's S_T. This suggests that a temperature gradient induces separation between PLL and ATP, with ATP migrating further from the hot region, resulting in an ATP-rich cold side and an ATP-depleted hot side (similar to the electrophoretic redistribution that drives the droplet toward the cathode, Figure 4b,c).

As in the interpretation for electrophoresis, the spatial redistribution of polyelectrolytes appears to be critical to droplet thermophoresis, with ion shielding at higher salt concentrations facilitating the more pronounced thermal migration of polyelectrolytes. Literature on temperature- and salt-dependent LLPS of charge-complexed coacervates indicates that stronger network interactions between polyelectrolytes form more solid-like, viscous, and thermally stable droplets.[13,15,35,52] From the compositional variation in both electrophoresis and thermophoresis, it can be inferred that the ATP-depleted condition lowers the interfacial tension compared to the ATP-enriched condition. Since high polyelectrolyte concentrations are a prerequisite for LLPS,[13] the depletion of ATP in the hot region shifts the local equilibrium toward a single solution phase, reducing interfacial tension and generating interfacial flows that drive thermophilic motion. This effect becomes more pronounced at high salt concentrations (Figure 4b,c). Further evidence comes from ATP concentration-dependent thermophoresis experiments (Figure S11), where the thermophoretic drift speed increased with the ATP concentration. No thermal motion was observed at the lowest concentration (2.5 mM), below which LLPS did not occur. As ATP has a higher S_T than that of PLL, its motion predominantly influences the compositional variation. Consequently, increased concentrations of ATP within a droplet create larger compositional and interfacial tension gradients, promoting a stronger Marangoni flow.

To demonstrate the effect of the composition gradient on the thermophoretic speed, fluid dynamics was simulated with a modified model. The thermophoretic motion in our system strongly relies on Marangoni flow, which is proportional to the interfacial tension gradient along the surface of the droplet. The interfacial tension can be described as $\gamma = \gamma_0 + \Delta\gamma_T + \Delta\gamma_n$, where γ_0 is the reference interfacial tension, and $\Delta\gamma_T$ and $\Delta\gamma_n$ are the variation in interfacial tension with thermal perturbation and composition effects, respectively. Since the composition gradient is governed by the thermal migration of ATP, $\mathrm{d}(\Delta\gamma_n) = \left(\frac{\partial\gamma}{\partial n_{\mathrm{ATP}}}\right)\mathrm{d}n_{\mathrm{ATP}} = \left(\frac{\partial\gamma}{\partial n_{\mathrm{ATP}}}\right)\left(\frac{\partial n_{\mathrm{ATP}}}{\partial T}\right)\mathrm{d}T = K_n\mathrm{d}T$, where the ATP concentration, n_{ATP}, is a function of temperature, T. The thermally driven ATP concentration gradient was empirically estimated by matching the simulated flow speed with the measured drift speed (see Note S3 and Figure S15 for details). Figures 5a–c show the simulated temperature, relative concentration, and flow profiles along the droplet surface, respectively (same geometry model as in Figure 4a). Given the temperature profile, n_{ATP} distributes along the surface in the opposite way, indicating the thermophobic migration of ATP. Strong Marangoni flows are induced at the lower hemisphere in the radial direction from the light source at the origin while leaving a quiet zone at the south pole due to the minimal tangential temperature and composition gradients. As shown in Figure 5d, the simulated thermophoretic drift speed depends linearly on the derived K_n, which is proportional to the ATP concentration gradient with respect to temperature, $\partial n_{\mathrm{ATP}}/\partial T$, the dominant factor of the thermally driven compositional Marangoni effect.

The thermophilic behavior of heat-dissociative coacervate droplets has the following implications in the quest to

https://doi.org/10.1021/acs.nanolett.4c03058
Nano Lett. 2024, 24, 15964−15972

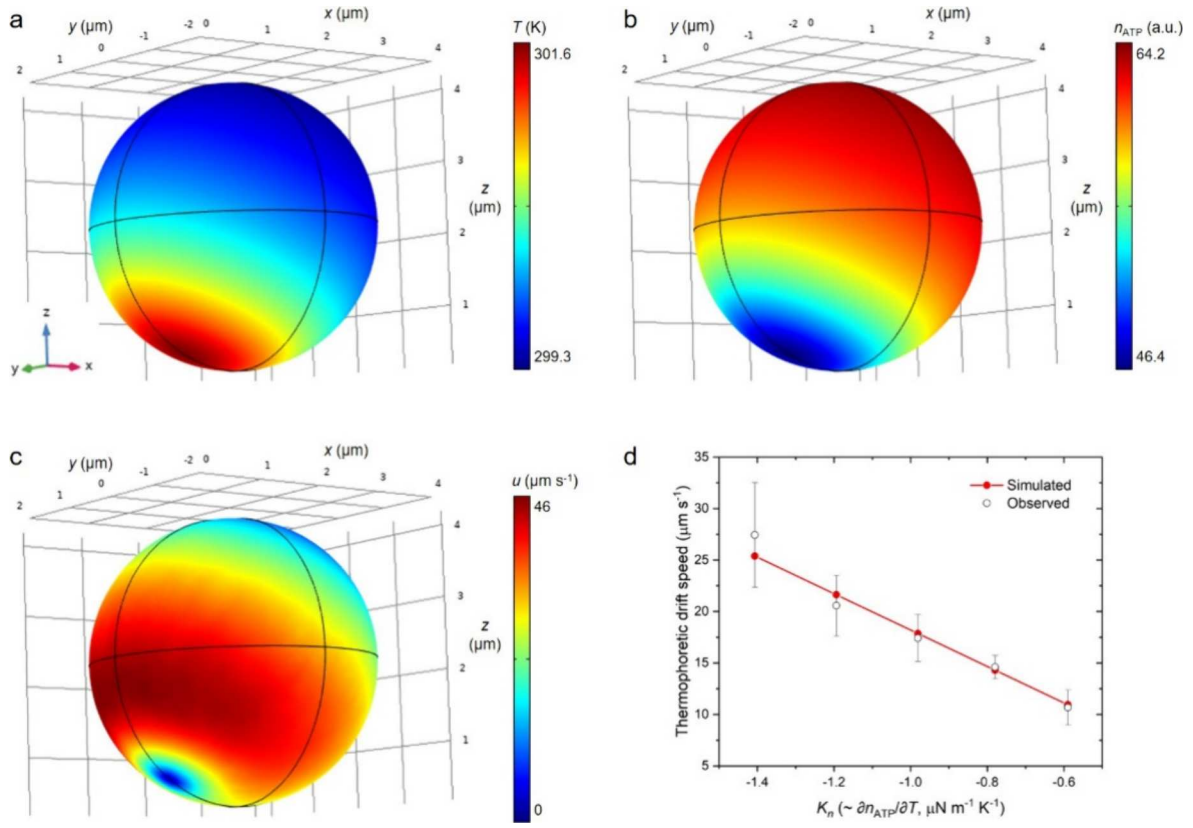

Figure 5. 3D surface plots of (a) temperature, (b) ATP concentration, and (c) velocity magnitude, u, along the droplet surface at a laser power of 0.51 mW. The droplet's position is the same as in Figure 4a, with the laser beam focused at the origin (0, 0, 0). (d) Simulated and observed thermophoretic drift speeds as a function of K_n, which is proportional to $\partial n_{ATP}/\partial T$. The observed thermophoretic speeds are adapted from Figure 2a.

understand the origin of life. Within the context of the deep-ocean hydrothermal hypothesis, LLPS-driven droplets would emerge from warm, molecule-rich fluids around the hydrothermal vents. Our initial intuition directs early condensates in these environments to be heat-associative. However, our study reveals that heat-dissociative coacervate droplets move against temperature gradients and preferentially reside in hotter zones. Considering that primordial molecular condensates might be loosely complexed and heat-dissociative with relatively short and simple macromolecules, our findings suggest their preferential existence near the vents, thus potentially accelerating the evolution of cellular forms through enhanced molecule accommodation and biochemical reactions. Moreover, our research has revealed that the separation of polyelectrolytes within droplets along a temperature gradient, in conjunction with the resulting interfacial flows, is crucial to determining both thermophoretic and electrophoretic behavior. This discovery challenges the conventional methods used to interpret the electrophoresis of coacervate droplets, which typically correlates their surface charge with the zeta potential under the solid-particle assumption. We believe that our study provides insights into the fate of biomolecular condensates in thermal landscapes at the beginning of life as well as a deeper understanding of the molecular nature of coacervate droplets, ultimately bridging the hydrothermal hypothesis on prebiotic synthesis with the condensate-as-protocell hypothesis related to cellular structuring.

■ ASSOCIATED CONTENT

Supporting Information

The Supporting Information is available free of charge at https://pubs.acs.org/doi/10.1021/acs.nanolett.4c03058.

Methods, summary of tested coacervate samples and their properties, UV−vis spectra of ATP, structural and optical properties of plasmonic substrates, optical microscopic images of coacervate droplets under various conditions, optical setup, turbidity, size and composition dependence of thermophoretic drift speed of PLL-ATP droplets, electrophoretic mobility of PDDA-ATP droplets, simulated temperature profiles, note for temperature-dependent physical properties of PLL-ATP coacervate phase, and derivation details for Soret coefficients of PLL and ATP (PDF)

Thermophoretic trapping and transport of PLL-ATP droplets (MP4)

Fusion and growth of PLL-ATP droplets under continuous laser exposure (MP4)

Thermal repelling of PDDA-ATP droplets (MP4)

Behavior of PLL-ATP droplets under an optical field (MP4)

Substrate adhesion of PLL-ATP droplets under an optothermal field at low salt concentrations (MP4)

■ AUTHOR INFORMATION

Corresponding Author

Yuebing Zheng − *Materials Science and Engineering Program, Texas Materials Institute, The University of Texas at Austin,*

https://doi.org/10.1021/acs.nanolett.4c03058
Nano Lett. 2024, 24, 15964−15972

Austin, Texas 78712, United States; Walker Department of Mechanical Engineering, The University of Texas at Austin, Austin, Texas 78712, United States; orcid.org/0000-0002-9168-9477; Email: zheng@austin.utexas.edu

Author

Youngsun Kim − *Materials Science and Engineering Program, Texas Materials Institute, The University of Texas at Austin, Austin, Texas 78712, United States; Chemical and Biological Integrative Research Center, Korea Institute of Science and Technology, Seoul 02792, Republic of Korea;* orcid.org/0000-0001-5219-8408

Complete contact information is available at: https://pubs.acs.org/10.1021/acs.nanolett.4c03058

Author Contributions

Y.K. and Y.Z. conceptualized the study. Y.K. conducted experiments and data analyses. Y.K. and Y.Z. wrote the manuscript. Y.Z. supervised the study. The manuscript was written through contributions of all authors. All authors have given approval to the final version of the manuscript.

Notes

The authors declare no competing financial interest.

■ ACKNOWLEDGMENTS

The authors acknowledge the financial support of the National Science Foundation (NSF-ECCS-2001650) and the National Institute of General Medical Sciences of the National Institutes of Health (R01GM146962). This work was also supported by grants from Korea Institute of Science and Technology (2E33132) and the National Research Foundation of Korea (RS-2024-00407093).

■ REFERENCES

(1) Alberti, S.; Gladfelter, A.; Mittag, T. Considerations and Challenges in Studying Liquid-Liquid Phase Separation and Biomolecular Condensates. *Cell* **2019**, *176* (3), 419−434.
(2) Shimobayashi, S. F.; Ronceray, P.; Sanders, D. W.; Haataja, M. P.; Brangwynne, C. P. Nucleation Landscape of Biomolecular Condensates. *Nature* **2021**, *599* (7885), 503−506.
(3) Shin, Y.; Brangwynne, C. P. Liquid Phase Condensation in Cell Physiology and Disease. *Science* **2017**, *357* (6357), DOI: 10.1126/science.aaf4382.
(4) Matsuo, M.; Kurihara, K. Proliferating Coacervate Droplets as the Missing Link between Chemistry and Biology in the Origins of Life. *Nat. Commun.* **2021**, *12* (1), 1−13.
(5) Poudyal, R. R.; Pir Cakmak, F.; Keating, C. D.; Bevilacqua, P. C. Physical Principles and Extant Biology Reveal Roles for RNA-Containing Membraneless Compartments in Origins of Life Chemistry. *Biochemistry* **2018**, *57* (17), 2509−2519.
(6) Yin, Y.; Niu, L.; Zhu, X.; Zhao, M.; Zhang, Z.; Mann, S.; Liang, D. Non-Equilibrium Behaviour in Coacervate-Based Protocells under Electric-Field-Induced Excitation. *Nat. Commun.* **2016**, *7*, 1−7.
(7) Guo, W.; Kinghorn, A. B.; Zhang, Y.; Li, Q.; Poonam, A. D.; Tanner, J. A.; Shum, H. C. Non-Associative Phase Separation in an Evaporating Droplet as a Model for Prebiotic Compartmentalization. *Nat. Commun.* **2021**, *12* (1), DOI: 10.1038/s41467-021-23410-7.
(8) Ianeselli, A.; Tetiker, D.; Stein, J.; Kühnlein, A.; Mast, C. B.; Braun, D.; Dora Tang, T. Y. Non-Equilibrium Conditions inside Rock Pores Drive Fission, Maintenance and Selection of Coacervate Protocells. *Nat. Chem.* **2022**, *14* (1), 32−39.
(9) Oparin, A. I. *The Origin of Life*; Macmillan: New York, 1938.
(10) Dai, Y.; You, L.; Chilkoti, A. Engineering Synthetic Biomolecular Condensates. *Nat. Rev. Bioeng.* **2023**, *1* (7), 466−480.
(11) Wadsworth, G. M.; Zahurancik, W. J.; Zeng, X.; Pullara, P.; Lai, L. B.; Sidharthan, V.; Pappu, R. V.; Gopalan, V.; Banerjee, P. R. RNAs Undergo Phase Transitions with Lower Critical Solution Temperatures. *Nat. Chem.* **2023**, *15* (12), 1693−1704.
(12) Lin, Z.; Beneyton, T.; Baret, J. C.; Martin, N. Coacervate Droplets for Synthetic Cells. *Small Methods* **2023**, *2300496*, 1−26.
(13) Fisher, R. S.; Elbaum-Garfinkle, S. Tunable Multiphase Dynamics of Arginine and Lysine Liquid Condensates. *Nat. Commun.* **2020**, *11* (1), DOI: 10.1038/s41467-020-18224-y.
(14) Valdes-Garcia, G.; Gamage, K.; Smith, C.; Martirosova, K.; Feig, M.; Lapidus, L. J. The Effect of Polymer Length in Liquid-Liquid Phase Separation. *Cell Reports Phys. Sci.* **2023**, *4* (5), 101415.
(15) Lu, T.; Nakashima, K. K.; Spruijt, E. Temperature-Responsive Peptide-Nucleotide Coacervates. *J. Phys. Chem. B* **2021**, *125* (12), 3080−3091.
(16) Martin, W.; Baross, J.; Kelley, D.; Russell, M. J. Hydrothermal Vents and the Origin of Life. *Nat. Rev. Microbiol.* **2008**, *6* (11), 805−814.
(17) Monnard, P. A.; Walde, P. Current Ideas about Prebiological Compartmentalization. *Life* **2015**, *5* (2), 1239−1263.
(18) Mast, C. B.; Schink, S.; Gerland, U.; Braun, D. Escalation of Polymerization in a Thermal Gradient. *Proc. Natl. Acad. Sci. U. S. A.* **2013**, *110* (20), 8030−8035.
(19) Agerschou, E. D.; Mast, C. B.; Braun, D. Emergence of Life from Trapped Nucleotides? Non-Equilibrium Behavior of Oligonucleotides in Thermal Gradients. *Synlett* **2016**, *28* (1), 56−63.
(20) Farag, M.; Cohen, S. R.; Borcherds, W. M.; Bremer, A.; Mittag, T.; Pappu, R. V. Condensates Formed by Prion-like Low-Complexity Domains Have Small-World Network Structures and Interfaces Defined by Expanded Conformations. *Nat. Commun.* **2022**, *13* (1), 1−15.
(21) Rizvi, A.; Favetta, B.; Jaber, N.; Lee, Y.-K.; Jiang, J.; Idris, N. S.; Schuster, B. S.; Dai, W.; Patterson, J. P. Revealing Nanoscale Structure and Interfaces of Protein and Polymer Condensates via Cryo-Electron Microscopy. *Nanoscale* **2024**, *16* (35), 16706−16717.
(22) Koga, S.; Williams, D. S.; Perriman, A. W.; Mann, S. Peptide-Nucleotide Microdroplets as a Step towards a Membrane-Free Protocell Model. *Nat. Chem.* **2011**, *3* (9), 720−724.
(23) Folkmann, A. W.; Putnam, A.; Lee, C. F.; Seydoux, G. Regulation of Biomolecular Condensates by Interfacial Protein Clusters. *Science* **2021**, *373* (6560), 1218−1224.
(24) Xu, C.; Martin, N.; Li, M.; Mann, S. Living Material Assembly of Bacteriogenic Protocells. *Nature* **2022**, *609* (7929), 1029−1037.
(25) Linsenmeier, M.; Faltova, L.; Morelli, C.; Capasso Palmiero, U.; Seiffert, C.; Küffner, A. M.; Pinotsi, D.; Zhou, J.; Mezzenga, R.; Arosio, P. The Interface of Condensates of the HnRNPA1 Low-Complexity Domain Promotes Formation of Amyloid Fibrils. *Nat. Chem.* **2023**, *15* (10), 1340−1349.
(26) Lipiński, W. P.; Visser, B. S.; Robu, I.; Fakhree, M. A. A.; Lindhoud, S.; Claessens, M. M. A. E.; Spruijt, E. Biomolecular Condensates Can Both Accelerate and Suppress Aggregation of α-Synuclein. *Sci. Adv.* **2022**, *8* (48), DOI: 10.1126/sciadv.abq6495.
(27) Tayar, A. M.; Caballero, F.; Anderberg, T.; Saleh, O. A.; Cristina Marchetti, M.; Dogic, Z. Controlling Liquid-Liquid Phase Behaviour with an Active Fluid. *Nat. Mater.* **2023**, *22* (11), 1401−1408.
(28) Shen, Y.; Ruggeri, F. S.; Vigolo, D.; Kamada, A.; Qamar, S.; Levin, A.; Iserman, C.; Alberti, S.; George-Hyslop, P. S.; Knowles, T. P. J. Biomolecular Condensates Undergo a Generic Shear-Mediated Liquid-to-Solid Transition. *Nat. Nanotechnol.* **2020**, *15* (10), 841−847.
(29) Hester, E. W.; Carney, S.; Shah, V.; Arnheim, A.; Patel, B.; Di Carlo, D.; Bertozzi, A. L. Fluid Dynamics Alters Liquid-Liquid Phase Separation in Confined Aqueous Two-Phase Systems. *Proc. Natl. Acad. Sci. U. S. A.* **2023**, *120* (49), 1−9.
(30) Sun, Y.; Lau, S. Y.; Lim, Z. W.; Chang, S. C.; Ghadessy, F.; Partridge, A.; Miserez, A. Phase-Separating Peptides for Direct Cytosolic Delivery and Redox-Activated Release of Macromolecular Therapeutics. *Nat. Chem.* **2022**, *14* (3), 274−283.

(31) Choi, S.; Meyer, M. C. O.; Bevilacqua, P. C.; Keating, C. D. Phase-Specific RNA Accumulation and Duplex Thermodynamics in Multiphase Coacervate Models for Membraneless Organelles. *Nat. Chem.* **2022**, *14* (10), 1110−1117.
(32) Doan, V. S.; Alshareedah, I.; Singh, A.; Banerjee, P. R.; Shin, S. Diffusiophoresis Promotes Phase Separation and Transport of Biomolecular Condensates. *Nat. Commun.* **2024**, *15* (1), 7686.
(33) Agrawal, A.; Douglas, J. F.; Tirrell, M.; Karim, A. Manipulation of Coacervate Droplets with an Electric Field. *Proc. Natl. Acad. Sci. U. S. A.* **2022**, *119* (32), No. e2203483119.
(34) Welsh, T. J.; Krainer, G.; Espinosa, J. R.; Joseph, J. A.; Sridhar, A.; Jahnel, M.; Arter, W. E.; Saar, K. L.; Alberti, S.; Collepardo-Guevara, R.; Knowles, T. P. J. Surface Electrostatics Govern the Emulsion Stability of Biomolecular Condensates. *Nano Lett.* **2022**, *22* (2), 612−621.
(35) Williams, D. S.; Koga, S.; Hak, C. R. C.; Majrekar, A.; Patil, A. J.; Perriman, A. W.; Mann, S. Polymer/Nucleotide Droplets as Bio-Inspired Functional Micro-Compartments. *Soft Matter* **2012**, *8* (22), 6004−6014.
(36) Mason, A. F.; Buddingh, B. C.; Williams, D. S.; Van Hest, J. C. M. Hierarchical Self-Assembly of a Copolymer-Stabilized Coacervate Protocell. *J. Am. Chem. Soc.* **2017**, *139* (48), 17309−17312.
(37) Rashidi, M.; Zargartalebi, M.; Benneker, A. M. Mechanistic Studies of Droplet Electrophoresis: A Review. *Electrophoresis* **2021**, *42* (7−8), 869−880.
(38) Wang, H.; Kelley, F. M.; Milovanovic, D.; Schuster, B. S.; Shi, Z. Surface Tension and Viscosity of Protein Condensates Quantified by Micropipette Aspiration. *Biophys. Reports* **2021**, *1* (1), 100011.
(39) van Haren, M. H. I.; Visser, B. S.; Spruijt, E. Probing the Surface Charge of Condensates Using Microelectrophoresis. *Nat. Commun.* **2024**, *15* (1), DOI: 10.1038/s41467-024-47885-2.
(40) Lin, L.; Peng, X.; Mao, Z.; Wei, X.; Xie, C.; Zheng, Y. Interfacial-Entropy-Driven Thermophoretic Tweezers. *Lab Chip* **2017**, *17* (18), 3061−3070.
(41) Ali, S.; Prabhu, V. M. Characterization of the Ultralow Interfacial Tension in Liquid-Liquid Phase Separated Polyelectrolyte Complex Coacervates by the Deformed Drop Retraction Method. *Macromolecules* **2019**, *52* (19), 7495−7502.
(42) Ohshima, H. A Simple Expression for the Electrophoretic Mobility of Charged Mercury Drops. *J. Colloid Interface Sci.* **1997**, *189* (2), 376−378.
(43) Baygents, J. C.; Saville, D. A. Electrophoresis of Drops and Bubbles. *J. Chem. Soc. Faraday Trans.* **1991**, *87* (12), 1883−1898.
(44) Qin, J.; Priftis, D.; Farina, R.; Perry, S. L.; Leon, L.; Whitmer, J.; Hoffmann, K.; Tirrell, M.; De Pablo, J. J. Interfacial Tension of Polyelectrolyte Complex Coacervate Phases. *ACS Macro Lett.* **2014**, *3* (6), 565−568.
(45) Zhang, P.; Wang, Z. G. Interfacial Structure and Tension of Polyelectrolyte Complex Coacervates. *Macromolecules* **2021**, *54* (23), 10994−11007.
(46) Schmitt, M.; Stark, H. Marangoni Flow at Droplet Interfaces: Three-Dimensional Solution and Applications. *Phys. Fluids* **2016**, *28* (1), 1−20.
(47) Li, Y.; Diddens, C.; Prosperetti, A.; Lohse, D. Marangoni Instability of a Drop in a Stably Stratified Liquid. *Phys. Rev. Lett.* **2021**, *126* (12), 1−16.
(48) Li, Y.; Meijer, J. G.; Lohse, D. Marangoni Instabilities of Drops of Different Viscosities in Stratified Liquids. *J. Fluid Mech.* **2022**, *932*, 1−18.
(49) Kim, Y.; Ding, H.; Zheng, Y. Investigating Water/Oil Interfaces with Opto-Thermophoresis. *Nat. Commun.* **2022**, *13* (1), 3742.
(50) Liu, S.; Lin, L.; Sun, H. B. Opto-Thermophoretic Manipulation. *ACS Nano* **2021**, *15* (4), 5925−5943.
(51) Maeda, Y. T.; Tlusty, T.; Libchaber, A. Effects of Long DNA Folding and Small RNA Stem-Loop in Thermophoresis. *Proc. Natl. Acad. Sci. U. S. A.* **2012**, *109* (44), 17972−17977.
(52) Lu, T.; Spruijt, E. Multiphase Complex Coacervate Droplets. *J. Am. Chem. Soc.* **2020**, *142* (6), 2905−2914.

https://doi.org/10.1021/acs.nanolett.4c03058
Nano Lett. 2024, 24, 15964−15972